Dissipative magnetic breathers induced by time-modulated voltages

Alejandro O. Leon,[1] Marcel G. Clerc,[2] and Dora Altbir[1]
[1]*Departamento de Física, CEDENNA, Universidad de Santiago de Chile, USACH, Av. Ecuador 3493, Santiago, Chile*
[2]*Departamento de Física and Millennium Institute for Research in Optics, Facultad de Ciencias Físicas y Matemáticas, Universidad de Chile, Casilla 487-3, Santiago, Chile*

(Received 18 October 2018; published 17 December 2018)

During the last years, there has been a growing interest in the coupling between voltages and the magnetization of insulating nanostructures. Applied voltages can change the magnetic anisotropy of magnetic tunnel junctions and generate magnetization dynamics more efficiently than alternating magnetic fields and spin-polarized electric currents because it avoids the Joule dissipation. Here, we study the formation of dissipative breathers in nanomagnets forced by an oscillatory voltage. The breathers are localized states with an oscillatory envelope. The voltage frequency is close to twice the ferromagnetic resonance frequency. Numerical simulations reveal that the breathers can emit evanescent spin waves from their center in a dipolarlike shape when the voltage is above a certain threshold. Based on an amplitude equation, we explain the existence and behavior of these *voltage-induced breathing solitons*, while the anisotropic spin-wave emission corresponds to a spontaneous symmetry-breaking instability.

DOI: 10.1103/PhysRevE.98.062213

I. INTRODUCTION

The quest for a low power consumption manipulation of magnetic materials has attracted considerable interest during the last decades. Ferromagnetic systems possess natural frequencies, and therefore an efficient magnetization control can be obtained by inducing resonances with oscillatory magnetic fields, electric currents, and voltages. In the presence of time-varying currents or electromagnetic fields, the resonances that require less energy injection are the ferromagnetic resonance when the forcing frequency is similar to the natural one, and the parametric resonance when the forcing frequency is about twice the natural one. The last case is characterized by several instabilities, in which the magnetization trajectories deviate from their equilibrium orientation when the energy injection is above a threshold. Parametric resonances have been studied in nanomagnets as induced by microwave fields [1–8], spin and charge currents [9–13], acoustic waves [14], and voltages [15–20]. This last mechanism is based on a *voltage-controlled magnetic anisotropy*, an effect that has been observed in transition-metal-based multilayers [21–25] such as the one depicted in Fig. 1, semiconductors [26], magnetoelectric materials [27–29], and proposed in magnetic insulators and nonmagnetic metal bilayers with interfacial rare-earth atoms [30]. Voltages applied to insulating structures do not generate Joule dissipation, which renders them lower power consumption systems as compared to electric-current-driven ones. Furthermore, with the aim of enhancing the coupling between voltages and the magnetization, and reducing the switching errors, studies considering several materials [31–34] and electric-field-pulse shapes [35,36] have been conducted.

In thin films with lateral dimensions larger than about 100 nm, the magnetization typically exhibits spatial textures, such as domain walls [37,38], vortices [39–42], skyrmions [43–48], and linear and nonlinear spin waves [49], to mention a few. Among localized states, solitons are particle-like solutions characterized by a position, width, and speed, with a nontopological profile. When the solitons have an oscillatory profile, they are usually called *breathers*. Even if the formation of magnetic patterns is relevant in both applied and fundamental reasons, the magnetic textures induced by time-dependent voltages have not been systematically explored yet.

The aim of this work is to study localized states, or dissipative solitons, induced by time-varying voltages. Based on numerical simulations and the amplitude equation of the magnetization, we show that solitons in magnetic-tunnel junctions can exhibit two types of behaviors: they can be localized oscillations symmetric around the soliton core or can have an oscillatory envelope that emits spin waves in anisotropic fashion, as shown in Fig. 2, respectively. In either case, one of the magnetization components is constant in time, and the two others oscillate.

II. THEORETICAL DESCRIPTION OF A MAGNETIC TUNNEL JUNCTION

Let us consider the magnetization dynamics of an ultrathin ferromagnetic material, such as Fe, Co, Ni, and their alloys. The magnet is grown on the top of an insulating film (see Fig. 1) to prevent the electric current flow. The application of a voltage changes the energy of the magnetic atoms at the *metal-insulator* interface. The magnet has a subnanometer thickness to enhance the relative strength of the coupling between the magnetization and the voltage, which is an interface effect. Additional magnetic layers with fixed magnetization can be used to measure the state of the *free magnetization* film via the tunnel magnetoresistance. We write the magnetization

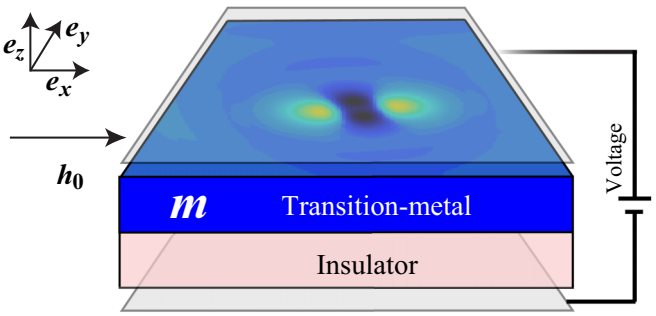

FIG. 1. Schematic representation of a magnetic tunnel junction with an applied voltage. The darker material is a transition-metal magnet, such as iron, cobalt, nickel, or their alloys. The thickness of the magnetic material is usually less than a nanometer to increase the relative importance of interface effects, such as the *voltage-controlled magnetic anisotropy* one. The insulator prevents the flow of charge current when voltages are applied. A typical insulator is MgO. The color map on the upper surface shows that the transition-metal layer typically exhibits well-localized textures, or *solitons*.

of the free film as $\mathbf{M} = M_s\mathbf{m}(t, \mathbf{r})$ in terms of its modulus M_s and the unit vector $\mathbf{m} = m_x\mathbf{e_x} + m_y\mathbf{e_y} + m_z\mathbf{e_z}$, where $\mathbf{e_j}$ is the Cartesian unitary vector along the axis j. The magnetization dynamics conserves its norm $|\mathbf{M}|^2 = M_s^2$. The spatial and temporal coordinates are rendered dimensionless by dividing by the characteristic scales $\mathbf{r} \equiv \mathbf{R}/l_{ex}$ and $t = T/t_c$, where $\mathbf{R}$ and T are the quantities with units, l_{ex} is the exchange length, and the temporal scale is $t_c = (|\gamma|M_s)^{-1}$, where γ is the gyromagentic ratio. For example, for 3-nm-thick cobalt, $l_{ex} = 3.4$ nm and $t_c = 3.2$ ps [51].

The dynamics of nanoscale ferromagnets is usually derived from a set of energies and their respective torques. We consider the following normalized energy E per unit of volume:

$$\frac{E}{\mu_0 M_s^2 V_0} = \int d^3r\left[-hm_x + \frac{\beta}{2}m_y^2 + \frac{\beta+\eta}{2}m_z^2\right], \qquad (1)$$

where the first term on the right-hand side is the Zeeman energy due to a magnetic field h pointing along the x axis. The second and third terms are the anisotropy energies for an ellipsoid body with principal axes along the respective Cartesian vectors. Constants β and η are combinations of demagnetizing factors and uniaxial magnetocrystalline anisotropy constants. The use of this local energy expression, instead of the full nonlocal demagnetizing energy (i.e., the *thin-film approximation*), is convenient in this work since we study the creation of textures, that are characterized by long times and slow dynamics. We normalized E by the shape anisotropy constant $\mu_0 M_s^2 V_0$, where μ_0 is the vacuum permeativity, and V_0 is the film volume. Using the norm conservation property $m_x^2 = 1 - m_y^2 - m_z^2$, we eliminated the explicit dependence on m_x^2. Notice that η accounts for the anisotropy in the (m_y, m_z) plane. In magnetic multilayers, the anisotropy constant η can depend on applied voltages [21–25,30] via the *voltage-controlled magnetic anisotropy (VCMA)* effect. As a result of this voltage dependence, an alternating electric field can switch the magnetization from one equilibrium to another in a precessional-like motion. The magnetization dynamics obeys [51]

$$\frac{\partial \mathbf{m}}{\partial t} = -\mathbf{m} \times [h\mathbf{e}_x - \beta m_y \mathbf{e}_y - (\beta+\eta)m_z\mathbf{e}_z]. \qquad (2)$$

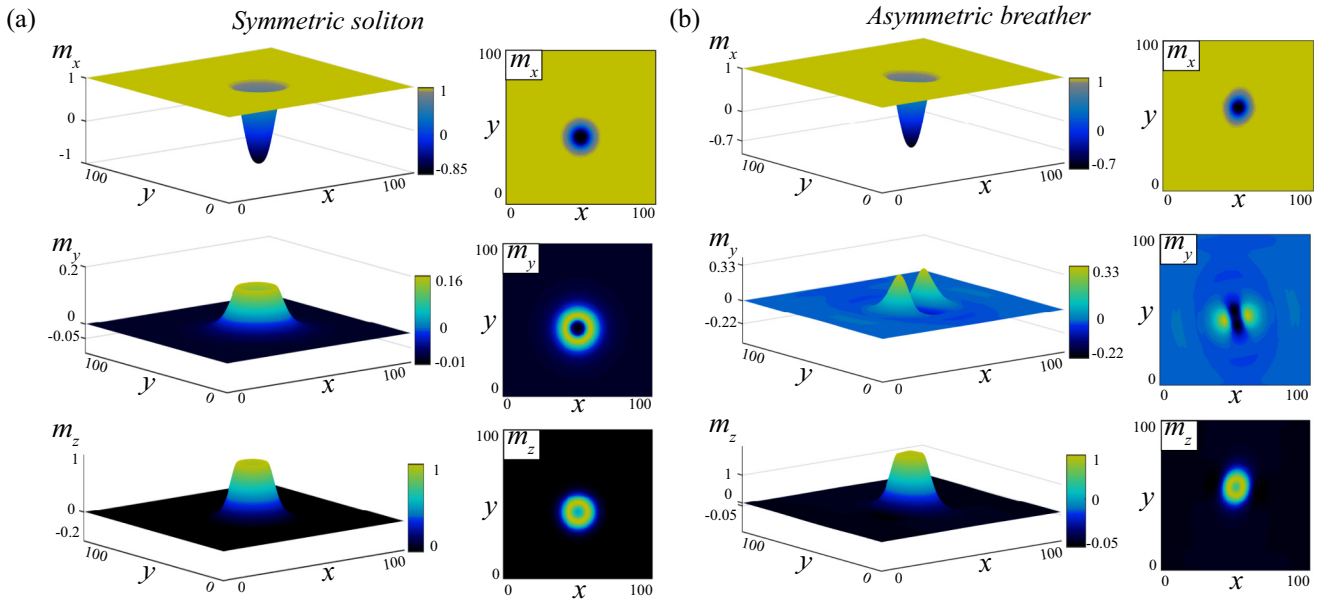

FIG. 2. Dissipative soliton and breather solutions for the magnetic tunnel junction with an applied voltage obtained from numerical simulations of LLG equation (4) with $\beta = 0$, $h = 1$, $\alpha = 0.05$, $\eta_0 = 0.2$, $\nu = -0.035$, $\delta\eta = 0.25$ (a), and $\delta\eta = 0.28$ (b). (a), (b) Account for symmetrical and asymmetrical localized solutions, respectively. The surfaces and their projected plots show the three components of the magnetization. The component m_x is almost constant in time and is saturated around $m_x = 1$ except by a hole, where $m_x \sim -0.85$ (a) and $m_x \sim -0.7$ (b). The other magnetization components oscillate with a half of the forcing frequency in a symmetric (a) and an asymmetric (b) fashion. Video with the temporal evolution of the dissipative soliton is available in the Supplemental Material [50].

For a strong magnetic field $h > 0$ (or equivalently $\beta > -\eta > 0$), the above equation describes an oscillator with an approximated solution given by

$$\begin{pmatrix} m_y \\ m_z \end{pmatrix} = A_0 e^{i\omega_0 t} \begin{pmatrix} \sqrt{h+\beta+\eta} \\ -i\sqrt{h+\beta} \end{pmatrix} + \text{c.c.}, \tag{3}$$

where $\omega_0 = \sqrt{(h+\beta)(h+\beta+\eta)}$ is the natural frequency and A_0 is a constant that depends on the initial conditions. The symbol c.c. stands for complex conjugate. The x component $m_x = [1-(m_y^2+m_z^2)]^{1/2}$ is a slave variable of (m_y, m_z) due to the norm conservation.

Beyond the conservative and uniform model described above, the exchange interaction energy in the continuum approach is $E_{\text{ex}}(\mu_0 M_s^2 V_0)^{-1} = \int d^3r |\nabla \mathbf{m}|^2/2$, and it induces a torque of the form $\mathbf{T}_{\text{ex}} = -\mathbf{m} \times \nabla^2 \mathbf{m}$, with $\nabla \equiv \mathbf{e_x}\partial_x + \mathbf{e_y}\partial_y$ being the gradient operator. Due to the small thickness of the magnet, we assume it to be uniformly magnetized along the z axis, $\partial_z \mathbf{m} \equiv 0$. The exchange torque favors uniform magnetic states. The system dissipation can be added as an extra torque, known as *Gilbert damping* $\mathbf{T}_{\text{d}} = \alpha \mathbf{m} \times (\partial \mathbf{m}/\partial t)$. This torque accounts for the energy transfers to the conduction electrons, lattice vibrations, and other degrees of freedom. The phenomenological parameter α is usually in the 10^{-4}–10^{-2} range [51].

To counterbalance the magnetic dissipation, we consider in the next section an oscillatory voltage. This voltage injects energy into the system in the form of a temporal modulation of the magnetic anisotropies. In particular, we consider $\eta(t) = \eta_0 + \delta\eta \cos(\Omega t)$, where η_0 and $\delta\eta$ are the constant and oscillatory components, respectively. It is known that parametrically driven systems exhibit instabilities when the forcing frequency is close to $\Omega = 2\omega_0/n$, where $n = 1, 2, 3, \ldots$ [52]. Furthermore, for systems with a small dissipation parameter $\alpha \ll 1$, the required energy injection at which the resonance occurs scales as $\alpha^{1/n}$ [52]. We focus here in the resonance with the smallest injection threshold, which occurs for $n = 1$. The corresponding forcing frequency $\Omega = 2(\omega_0 + \nu)$ is in the GHz range, and ν is a small detuning parameter. In experiments, the constant η_0 can be modulated by a constant voltage, as well as by the thickness of the ferromagnetic film. For example, FeCo has $\eta_0 \approx 0$ for a thickness of 0.54 nm [23], while $\eta_0 > 0$ ($\eta_0 < 0$) for larger (smaller) thicknesses.

We sum the aforementioned torques to obtain the total Landau-Lifshitz-Gilbert (LLG) equation [51]

$$\frac{\partial \mathbf{m}}{\partial t} = -\mathbf{m} \times [h\mathbf{e}_x - \beta m_y \mathbf{e}_y - [\beta + \eta(t)] m_z \mathbf{e}_z] - \mathbf{m} \times \left[\nabla^2 \mathbf{m} - \alpha \frac{\partial \mathbf{m}}{\partial t}\right], \tag{4}$$

that describes a driven and damped magnetic oscillator.

III. PARAMETRIC RESONANCE INDUCED BY ALTERNATING VOLTAGES

When a system is forced at about twice its natural frequency, it can exhibit a parametric instability. At the onset of this instability, chains of coupled oscillators exhibit intriguing dynamic behaviors such as Faraday waves [53,54], dissipative solitons [55–57], localized states with phase structures [58], breathers [59], domain walls [60], among others. One systematic strategy to investigate their dynamics is to characterize the envelope close to the resonance frequency. Let us introduce a perturbation from the simple solution of formula (3):

$$\begin{pmatrix} m_y \\ m_z \end{pmatrix} = A(t, \mathbf{r}) e^{i\omega_0 t} \begin{pmatrix} \sqrt{h+\beta+\eta_0} \\ -i\sqrt{h+\beta} \end{pmatrix} + \text{c.c.} + \mathbf{W}, \tag{5}$$

where $A(t, \mathbf{r})$ is a space-time-dependent amplitude. The function $\mathbf{W}$ is a higher-order correction $|\mathbf{W}| \ll |A| \ll 1$, that one needs to include to satisfy Eq. (4) at nonlinear orders. After straightforward calculations one obtains the equation for the envelope A (see details in Appendix A):

$$\partial_t A = -iC_0 A|A|^2 - i\kappa \nabla^2 A - \mu A + i\Gamma e^{2i\nu t} A^*, \tag{6}$$

which is known as the *parametrically-driven damped nonlinear Schrödinger* equation (PNDLS) [61]. The coefficient of the saturation is

$$C_0 \equiv (h+\beta)(\beta+\eta_0)(4h+4\beta+\eta_0)/(4\omega_0) + \beta(h+\beta+\eta_0)(4h+4\beta+3\eta_0)/(4\omega_0), \tag{7}$$

the parameter of the dispersion is $\kappa \equiv [2h+2\beta+\eta_0]/(2\omega_0)$. The term that accounts for the voltage-induced injection of energy is given by

$$\Gamma \equiv \frac{(\beta+h)\delta\eta}{4\omega_0}, \tag{8}$$

and the effective dissipation is

$$\mu \equiv \alpha\left(h+\beta+\frac{\eta_0}{2}\right). \tag{9}$$

Equation (6) can be further simplified by the change of variables $A(t, \mathbf{r}) = C_0^{-1/2} e^{i\nu t + \pi i/4} B(t, \mathbf{x})$, where $\mathbf{r} = \kappa^{1/2}\mathbf{x}$:

$$\partial_t B = -i(\nu + |B|^2 + \nabla'^2)B - \mu B + \Gamma B^*, \tag{10}$$

where $\nabla' \equiv \partial/\partial \mathbf{x}$. The above equation rules the envelope dynamics driven by voltages. The phenomenology of the PDNLS equation when the parametric forcing is a magnetic field or electric current can be found in Refs. [62,63] and references therein. We explore in the next subsections the localized solutions of Eq. (10).

A. Dissipative solitons at the onset of the parametric resonance

Let us start here by reviewing the soliton solution in one spatial dimension. Using polar decomposition $B = Re^{i\phi}$, where the modulus $R(t, x)$ and phase $\phi(t)$ obey

$$\partial_t R = -\mu R + \gamma R \cos(2\phi), \tag{11}$$

$$\partial_t \phi = -\nu - R^2 - R^{-1}\partial_{xx} R - \gamma \sin(2\phi). \tag{12}$$

The above model has dissipative soliton solution of the form [64]

$$\cos(2\phi_s) = \mu/\gamma, \quad R_s(x) = \sqrt{2\Delta}\,\text{sech}(\sqrt{\Delta}x), \tag{13}$$

where $\Delta \equiv -\nu - \sqrt{\gamma^2 - \mu^2}$. Figure 3(a) shows this localized state. Notice that this function is real only when the voltage-induced energy injection surpasses the magnetic dissipation $\gamma \geqslant \mu$. In addition, the forcing frequency must be smaller than twice the natural one, $2\omega_0 - \Omega = -2\nu > 2\sqrt{\gamma^2 - \mu^2}$.

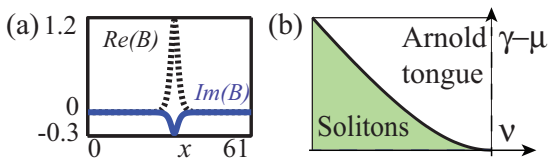

FIG. 3. One-dimensional dissipative soliton. (a) Soliton state in the complex envelope, where $\mathrm{Re}(B)$ and $\mathrm{Im}(B)$ stand for the real and imaginary parts of B, respectively, obtained for $\gamma = -\nu = \frac{1}{2}$, $\mu = 0.45$. (b) The solitons exist when $\gamma > \mu$, that is, the injected energy is larger than the dissipated one; and $-\nu > \sqrt{\gamma^2 - \mu^2}$ (on the left of the so-called Arnold-tongue zone).

Figure 3(b) depicts in the parameter space darker (green online) zone of soliton solutions. Once the region of the parameter space where this solution exists is determined, one can search for it using direct numerical simulations of the LLG equation, with the numerical method described in Appendix B. It is worth mentioning that in the region where solitons exist, the uniform state $\mathbf{m} = \mathbf{e_x}$ (ferromagnetic state) is also stable. Then, depending on the initial condition, the system can reach any of the two possible solutions. Figure 4(a) shows the magnetization components of a soliton state in one spatial dimension. When the injection of energy is larger and the detuning is more negative, the soliton envelope starts to oscillate pumping spin waves with a breathinglike fashion [see Fig. 4(b)]. These breather states have been reported in several systems with one spatial dimension (see Ref. [65] and references therein). On the other hand, to the best of our knowledge, their two-dimensional counterparts have not been reported. Furthermore, the analytic solution for the symmetric soliton is unknown in two dimensions. Approximations based on hyperbolic functions can be found in Ref. [66].

IV. VOLTAGE-INDUCED TWO-DIMENSIONAL BREATHERS

Numerical simulations of the LLG equation (4) close to parametrical instability exhibit oscillatory dissipative solitons. Figure 2(a) shows the typical observed solitons for the magnetic tunnel junction with an applied voltage ($\delta\eta = 0.25$).

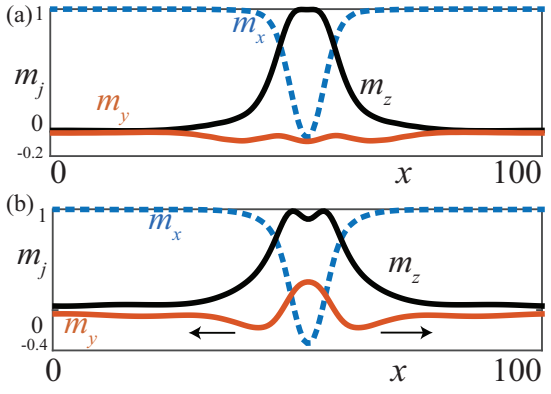

FIG. 4. Snapshot of the localized states for $h = 1$, $\alpha = 0.05$, $\beta = 0$, $\nu = -0.035$, $\eta_0 = 0.2$. (a) Soliton with monotonic-decaying envelope, and $\delta\eta = 0.25$. (b) Soliton with oscillatory-decaying envelope, or breather, for $\delta\eta = 0.28$.

Note that this solution is symmetric, and characterized by the emission of circular evanescent waves. The component m_x is saturated around the $m_x = 1$ value, except in a small central region where it has a hole and m_x reaches ≈ -0.7. The m_y and m_z components oscillate in a ringlike fashion. The form of the oscillation is due to the norm conservation $m_x^2 + m_y^2 + m_z^2 = 1$, and that $|m_x|$ is large in both the central region and outside the soliton. Then, m_y and m_z can be large only in the ring-type region where $m_x \approx 0$. For this figure, we use the following set of parameters: $h = 1$, $\beta = 0$, $\eta_0 = 0.2$, $\delta\eta = 0.25$, $\alpha = 0.05$, and $\nu = -0.035$. The corresponding parameters of the amplitude equation are $\Gamma = 0.0571$ and $\mu = 0.055$.

Counterintuitively, when increasing the amplitude of the voltage, the solution becomes asymmetric as it is illustrated in Fig. 2(b). This soliton solution has an oscillatory envelope (breathinglike mode) that is usually known as *breather*. The breather is asymmetric and is characterized by having two dominant lobes. The orientation of the lobes is determined by the initial conditions. These breathing solutions are characterized by the radiation of evanescent waves with a dipolar structure. Hence, increasing the amplitude of the voltage oscillation, the magnetic film exhibits a transition between a symmetric soliton and an asymmetric breather.

Breathers are commonly observed in one-dimensional parametrically driven systems. Their existence in two-dimensional systems, to the best of our knowledge, has not been reported before. This could be due to the uniqueness of magnetic tunnel junctions to modulate both the linear and nonlinear effects via an applied voltage.

To characterize the level of asymmetry of the breather solutions, one can compare the difference between the magnetization profiles along the x and y axes [see Fig. 5(a)]:

$$\delta(t;\Gamma) \equiv \max_s |m_y(t, \mathbf{r_0} + s\mathbf{e_x}) - m_y(t, \mathbf{r_0} + s\mathbf{e_y})|, \quad (14)$$

where the maximum value is calculated for distances $2dx \leqslant \delta \leqslant 50dx$, where dx is the spatial step size of the simulations. Figure 5(c) depicts the temporal evolution of the $\delta(t;\Gamma)$. Clearly, this quantity exhibits a periodic behavior. The Fourier transform of this temporal signal exhibits a well-defined frequency and its harmonics [see Fig. 5(d)]. In addition, taking the maximum over time, one gets a global indicator

$$\Delta(\Gamma) \equiv \max_t [\delta(t;\Gamma)], \quad (15)$$

which quantifies the degree of asymmetry of the solutions as a function of the alternating voltage (effective) parameter Γ. Figure 5(b) shows this curve. As we can see, there is a continuous or supercritical transition between the symmetric and the asymmetric states. Indeed, this transition corresponds to the spontaneous breaking of rotation symmetry of the breather solution.

From the viewpoint of nanomagnetism, we see that anisotropic solutions have larger gradients compared to the isotropic ones since they involve nonuniformities in both the radial and the angular coordinates. Thus, anisotropic breathers have larger exchange energies and are stable only when the energy injection is above a threshold. From the above numerical results, we can conclude that the symmetric breather suffers an instability in which an asymmetric oscillatory mode

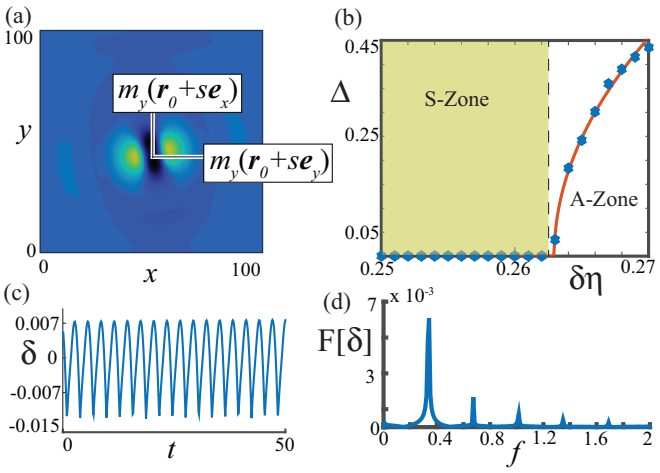

FIG. 5. Asymmetric breather solution. (a) Schematic representation of the dynamical indicator to measure the asymmetry level of the breather solution, which is the difference between trajectories around the soliton core, $\delta(t,s;\Gamma) \equiv |m_y(\mathbf{r_0}+s\mathbf{e}_x,t) - m_y(\mathbf{r_0}+s\mathbf{e}_y,t)|$. (b) Bifurcation diagram of the solitons, where we plot the maximum value of δ for each value of the Γ parameter. In the S zone, the localized state is centrosymmetric, while in the A region, the soliton emits asymmetric waves. The dots are numerical results, while the curve is the fitting $\Delta(\delta\eta) = 5.421\sqrt{\delta\eta - 0.2629}$. (c), (d) Show the temporal and Fourier series of $\delta(t)$, respectively, for $\delta\eta = 0.263$. The dominant frequency of the spectrum is for $f = 0.332$ which is about twice the soliton frequency (0.166). Then, the period of the asymmetric oscillation is $T = 1/f = 3$.

emerges. The amplitude of the instability mode grows continuously as a function of the injected energy parameter Γ. From the dynamical systems point of view, we can identify the transition as a *supercritical Andronov-Hopf instability with a nonuniform critical mode*. The analytic treatment of this instability is a difficult task because the amplitude of the breathers is not small and does not allow a perturbation treatment. It is still possible to develop an understanding from symmetry arguments, as follows. Any initial condition around the soliton solution $m_y^{(S)}$ and $m_z^{(S)}$ can be decomposed as

$$\begin{pmatrix} m_y \\ m_z \end{pmatrix} = \begin{pmatrix} m_y^{(S)} \\ m_z^{(S)} \end{pmatrix}(t,\mathbf{r}) + \delta\mathbf{m}, \tag{16}$$

where $\delta\mathbf{m}$ is a small perturbation that obeys $\partial_t\delta\mathbf{m} = \mathbb{L}\delta\mathbf{m}$, where $\mathbb{L} = \mathbb{L}(m_y^{(S)}, m_z^{(S)}, \nabla^2 m_y^{(S)}, \nabla^2 m_z^{(S)})$ is the Jacobian of the LLG equation evaluated on the soliton solution and its gradients. The general solution of the perturbation reads as

$$\delta\mathbf{m}(t,\mathbf{r}) = \sum_j \psi_j e^{\lambda_j t}\mathbf{v}_j(t,\mathbf{r}) + \text{c.c.}, \tag{17}$$

where ψ_j is the amplitude fixed by the initial condition, λ_j are the Lyapunov exponents, and $\mathbf{v}_j$ are the corresponding functions. When one of the Lyapunov exponents has a positive real part $\lambda_0 \geqslant 0$, then the mode grows and the linear equation is no longer valid. In this case, the amplitude of the growing mode ψ is rendered a dynamical quantity. When $|\psi| \ll 1$ and it preserves its phase variance (i.e., the voltage-induced oscillation expresses only in the critical mode $\mathbf{v}_0$), then complex field ψ obeys the so-called Ginzburg-Landau equation

$$\partial_t\psi = \lambda_0\psi - (c_1 + ic_2)\psi|\psi|^2, \tag{18}$$

where we can decompose $\lambda_0 = \epsilon_R + i\epsilon_I$. The coefficient ϵ_R is related to the energy injection and dissipation and c_1 accounts for the saturation (nonlinear dissipation effects). The linear and nonlinear frequency shifts are given by ϵ_I and c_2, respectively. The solutions of the above model are $\psi = 0$ for $\epsilon_R < 0$, and

$$\psi = \sqrt{\frac{\epsilon_R}{c_1}}e^{i(\epsilon_I - \epsilon_R\frac{c_2}{c_1})t} \tag{19}$$

for $\epsilon > 0$. Note that the dynamical indicator Δ is related to the mode ψ via

$$\Delta = \max_{t,s}|\psi[\mathbf{v}_{0,y}(t,\mathbf{r_0}+s\mathbf{e_x}) - \mathbf{v}_{0,y}(t,\mathbf{r_0}+s\mathbf{e_y})]| \tag{20}$$

$$= \sqrt{\frac{\epsilon_R}{c_1}}g_0, \tag{21}$$

where the parameter $g_0 = \max_{t,s}|\mathbf{v}_{0,y}(t,\mathbf{r_0}+s\mathbf{e_x}) - \mathbf{v}_{0,y}(t,\mathbf{r_0}+s\mathbf{e_y})|$ encodes all the information about the critical mode of the instability. Then, the phenomenological model proposed here is in agreement with the numerical simulations shown in Fig. 5, with $\epsilon_R = \delta\eta - 0.2629$. We cannot directly access the eigenfrequency ϵ_I or the nonlinear correction of the frequency $\epsilon_R c_2/c_1$ because the Fourier spectrum of the asymmetric mode reveals only that $\psi_0 e^{\lambda_0 t}\mathbf{v}_0(t,\mathbf{r})$ oscillates at (nearly) twice the soliton frequency. Thus, the instability occurs approximately at the forcing frequency.

Let us estimate here the physical parameter values that characterize the soliton and breather states. Considering a 3-nm-thick cobalt, $l_{ex} = 3.4$ nm and $t_c = 3.2$ ps, and using the symmetries of the LLG equation shown in Appendix B (with $\xi = \frac{1}{10}$), the natural and forcing frequencies (one divided by the period) are $\omega_0\xi \sim 5$ GHz and $f_F\xi \sim 10$ GHz, respectively. The field is $h\xi = \frac{1}{10}$, and for a saturation magnetization of $\mu_0 M_s = 1.82$ T, the field with units is about $M_s h\xi = 0.18$ T. The typical soliton radius (i.e., radius of the $|m_x| \approx 0$ curve) for these parameters is about 120 nm. Let us stress that using the stability conditions of Fig. 3 together with Eqs. (8) and (9), one can find the necessary alternating voltage and frequency detuning to observe breathers in a system with a different set of applied field and anisotropy constant parameters.

V. CONCLUSIONS AND REMARKS

The *voltage-controlled magnetic anisotropy* effect is a forcing mechanism that can produce magnetic reversions and ferromagnetic resonances with a relatively low power consumption. Then, this mechanism is a promising candidate for memory technologies. Beyond the magnetization dynamics relevant to applications, voltages are capable of producing a strong response in magnets since they modulate the nonlinear effects. Here, we have shown that a voltage oscillating at about twice the magnet natural frequency is capable of producing parametric instabilities and localized states. Those localized states can have both a stationary and an oscillatory envelope. In the last case, the soliton center emits spin waves in an anisotropic fashion. The transition between the isotropic and

anisotropic states is a supercritical oscillatory instability. The existence of such solutions is possible due to the *quasi*-Hamiltonian nature of ferroferrimagnetic systems and the possibility to manipulate the parameters of both the linear and nonlinear terms in the LLG equation. These attributes make this system ideal to study nonlinear dynamics.

ACKNOWLEDGMENTS

A.O.L. and D.A. acknowledge financial support in Chile from Financiamiento Basal para Centros Científicos y Tecnológicos de Excelencia FB 0807. We also acknowledge support from Fondecyt under Grants No. 1160198 and No. 1180903. M.C. acknowledges financial support from the Millennium Institute for Research in Optics (MIRO).

APPENDIX A: DERIVATION OF THE AMPLITUDE EQUATION

In this appendix, we consider a voltage with a constant and an oscillatory part $\eta(t) = \eta_0 + \delta\eta\cos(\Omega t)$, and derive the equation for the magnetization oscillation envelope. In this calculation, the parameters that account for the injection and dissipation of energy obey the scaling $|\delta\eta/\eta_0| \sim \alpha \ll 1$, that is necessary for a perturbation approach. The other parameters are assumed to be of order one, $h \sim \beta \sim \eta_0 \sim 1$. Let us consider the dynamics of the small and spatially slow transverse components m_y and m_z:

$$m_y^2 \sim m_z^2 \sim \left|\frac{\nabla^2 m_y}{m_y}\right| \sim \left|\frac{\nabla^2 m_z}{m_z}\right| \ll 1. \tag{A1}$$

This is not necessarily a good quantitative approximation for all values of η_0 and $\delta\eta$; however, it serves to derive a model with qualitative validity. Using the above scaling, and after straightforward calculations, the LLG equation can be simplified to

$$\frac{\partial}{\partial t}\begin{pmatrix} m_y \\ m_z \end{pmatrix} \approx \left[\mathbb{M}_{\omega_0} + \mathbb{M}_\nabla + \mathbb{M}_{\rm NL} + \mathbb{M}_{\rm osc} + \mathbb{M}_{\rm D}\right]\begin{pmatrix} m_y \\ m_z \end{pmatrix}. \tag{A2}$$

Let us review in the following each one of the matrices. The dominant part of Eq. (A2) is given by

$$\mathbb{M}_{\omega_0} \equiv \begin{bmatrix} 0 & -h-\beta-\eta_0 \\ h+\beta & 0 \end{bmatrix}, \tag{A3}$$

which accounts for the linear conservative effects. Nonlinearities arise from the magnetic anisotropies

$$\mathbb{M}_{\rm NL}(m_y, m_z) \equiv \frac{m_y^2 + m_z^2}{2}\begin{bmatrix} 0 & \beta+\eta_0 \\ -\beta & 0 \end{bmatrix}, \tag{A4}$$

while the exchange matrix is

$$\mathbb{M}_\nabla \equiv \begin{bmatrix} 0 & 1 \\ -1 & 0 \end{bmatrix}\nabla^2. \tag{A5}$$

The dissipative effects are summarized in the matrix

$$\mathbb{M}_{\rm D} \equiv -\begin{bmatrix} \alpha(h+\beta) & 0 \\ 0 & \alpha(h+\beta+\eta_0) \end{bmatrix}. \tag{A6}$$

The oscillatory effects contribute as

$$\mathbb{M}_{\rm osc} \equiv \cos(\Omega t)\begin{bmatrix} 0 & -\delta\eta \\ 0 & 0 \end{bmatrix}. \tag{A7}$$

The parametric instability takes place when $\Omega = 2(\omega_0 + \nu)$, where ν is a small detuning $|\nu|/\omega_0 \ll 1$. Let us introduce the following change of variables:

$$\begin{pmatrix} m_y \\ m_z \end{pmatrix} = Ae^{i\omega_0 t}\mathbf{u} + \text{c.c.} + \mathbf{W}, \tag{A8}$$

where the amplitude A varies slowly in time and space, $|\nabla^2 A| \sim |\partial_t A| \ll |A| \ll 1$, and the vector $\mathbf{u}$ is

$$\mathbf{u} \equiv \begin{pmatrix} \sqrt{h+\beta+\eta_0} \\ -i\sqrt{h+\beta} \end{pmatrix}. \tag{A9}$$

This ansatz is a perturbation of the system state obtained when $\delta\eta = \alpha = |\nabla^2\mathbf{m}| = 0$, given by Eq. (3). Due to the nonlinear nature of Eq. (A2), a function of the form $Ae^{i\omega_0 t}\mathbf{u}$ cannot be a solution of the system. We need then to promote the A_0 constant of formula (3) to a space-time-dependent field and add a nonlinear correction to the solution

$$\mathbf{W} = \mathbf{W}(A, A^*, \nabla^2 A, \nabla^2 A^*, t).$$

The function $\mathbf{W}$ is a higher-order correction to be found later, and it might scale as $|\mathbf{W}| \sim |A|^3$. Replacing the ansatz (5) in Eq. (A2), and linearizing around the correction $\mathbf{W}$, one obtains

$$\begin{aligned}\hat{L}\mathbf{W} = {} & [\partial_t A - gA]e^{i\omega_0 t}\mathbf{u} + (\nabla^2 - i\alpha\omega_0) \\ & \times Ae^{i\omega_0 t}\begin{pmatrix} i\sqrt{h+\beta} \\ \sqrt{h+\beta+\eta_0} \end{pmatrix}\frac{i\sqrt{h+\beta}\delta\eta}{2} \\ & \times A^* e^{2i\nu t}e^{i\omega_0 t}\begin{pmatrix} 1 \\ 0 \end{pmatrix} + \text{c.c.} \\ & + \frac{1}{2}A|A|^2 e^{i\omega_0 t}\begin{pmatrix} i(\beta+\eta_0)(4h+4\beta+\eta_0)\sqrt{h+\beta} \\ \beta_0(4h+4\beta+3\eta_0)\sqrt{h+\beta+\eta_0} \end{pmatrix} \\ & + A^3 e^{3i\omega_0 t}\mathbf{f}_c, \end{aligned} \tag{A10}$$

where

$$\hat{L} \equiv \mathbb{M}_{\omega_0} - \partial_t = \begin{bmatrix} -\partial_t & -h-\beta-\eta_0 \\ h+\beta & -\partial_t \end{bmatrix}, \tag{A11}$$

and the function $\mathbf{f}_c$ contains all the constants of the cubic term $A^3 e^{3i\omega_0 t}$. Notice that in the above equation both the nonlinear function $\mathbf{W}$ and the evolution of the envelopes $\partial_t A$ and $\partial_t A^*$ are unknown. By the Freedholm alternative, Eq. (A10) can be solved (for $\mathbf{W} \neq \mathbf{0}$) if its right-hand side is orthogonal to the elements of the kernel of the adjoint operator $\hat{L}^\dagger$. We define the inner product of functions space

$$(\mathbf{a}, \mathbf{b}) \equiv \frac{\omega_0}{2\pi}\int_{t_0}^{t_0+2\pi/\omega_0} (\mathbf{a}^* \cdot \mathbf{b})dt, \tag{A12}$$

where the center dot denotes the inner product of vectors with complex components, i.e., the dot product of $\mathbb{C}^2$. Then, the adjoint operator $\hat{L}^\dagger$ is

$$\hat{L}^\dagger = \begin{bmatrix} \partial_t & h+\beta \\ -h-\beta-\eta_0 & \partial_t \end{bmatrix},$$

and its kernel is given by the vectors $e^{\pm i\omega_0 t}(\pm i\sqrt{h+\beta}, \sqrt{h+\beta+\eta_0})^T$. Using Freedholm

alternative, the aptitude A obeys (the PNDLS [61])

$$\partial_t A = -iC_0 A|A|^2 - i\kappa\nabla^2 A - \mu A + i\Gamma e^{2i\nu t}A^*, \quad \text{(A13)}$$

where

$$4\omega_0 C_0 = (h+\beta)(\beta+\eta_0)(4h+4\beta+\eta_0) + \beta(h+\beta+\eta_0)(4h+4\beta+3\eta_0), \quad \text{(A14)}$$

$$\kappa = \frac{2h+2\beta+\eta_0}{2\omega_0}, \quad \text{(A15)}$$

$$\Gamma = \frac{(\beta+h)\delta\eta}{4\omega_0}, \quad \text{(A16)}$$

$$\mu = \alpha\left(h+\beta+\frac{\eta_0}{2}\right). \quad \text{(A17)}$$

APPENDIX B: NUMERIC METHOD

Let us start recalling that the Landau-Lishitz-Gilbert model (4) is invariant under transformation of the form $\{\partial_t, \nabla^2; h, \beta, \eta\} \to \{\xi\partial_t, \xi\nabla^2; \xi h, \xi\beta, \xi\eta\}$, where ξ is a real number. This is particularly useful when all parameters are small because we can use $\xi = h^{-1}$ and then obtain a much shorter simulation time.

Regarding the discretization of the spatial coordinates in one dimension, we write $x(i) = idx$, and then $\mathbf{m}_i(t) \equiv \mathbf{m}(t, idx)$, for a step size dx and position label i. The Laplacian of the magnetization can be approximated as [67]

$$dx^2 \cdot \partial_{xx}\mathbf{m}_i = \frac{1}{90}(\mathbf{m}_{i+3}+\mathbf{m}_{i-3}) - \frac{3}{20}(\mathbf{m}_{i+2}+\mathbf{m}_{i-2}) + \frac{3}{2}(\mathbf{m}_{i+1}+\mathbf{m}_{i-1}) - \frac{49}{18}\mathbf{m}_i + \frac{dx^8}{560}\frac{\partial^8\mathbf{m}_i}{\partial x^8}, \quad \text{(B1)}$$

where the last term is the discretization error. Notice that if $|\partial^8\mathbf{m}_i/\partial x^8| \sim 1$ and $\Delta x \sim 0.5$, then the error of the Laplacian expression is of order $dx^8(\partial^8\mathbf{m}_i/\partial x^8)/560 \sim 7\times 10^{-6}$, which is small enough for this study. Apart from the improved precision given by Eq. (B1), the results are the same when other discretization expressions and other dx values are considered. The two-dimensional discretization is analogous since $\nabla^2 = \partial_{xx} + \partial_{yy}$.

We found it useful to use the spherical representation of the magnetization

$$\mathbf{m} = \sin(\theta)[\cos(\phi)\mathbf{e_x} + \sin(\phi)\mathbf{e_y}] + \cos(\theta)\mathbf{e_z}, \quad \text{(B2)}$$

where the dynamical variables are the polar $\theta(\mathbf{r}, t)$ and azimuthal $\phi(\mathbf{r}, t)$ angles. This representation is convenient because the mapping (B2) preserves the magnetization norm, and we are far from the $\theta = 0$ and π poles. The set of $\{\theta_i(t), \phi_i(t)\}$ is then integrated in time using the fifth-order Runge-Kutta scheme of Ref. [68] with a constant temporal step size of $dt = 0.001$.

[1] S. Urazhdin, V. Tiberkevich, and A. Slavin, Parametric Excitation of a Magnetic Nanocontact by a Microwave Field, Phys. Rev. Lett. **105**, 237204 (2010).

[2] H. Ulrichs, V. E. Demidov, S. O. Demokritov, and S. Urazhdin, Parametric excitation of eigenmodes in microscopic magnetic dots, Phys. Rev. B **84**, 094401 (2011).

[3] F. Guo, L. M. Belova, and R. D. McMichael, Parametric pumping of precession modes in ferromagnetic nanodisks, Phys. Rev. B **89**, 104422 (2014).

[4] A. O. Leon, M. G. Clerc, and S. Coulibaly, Traveling pulse on a periodic background in parametrically driven systems, Phys. Rev. E **91**, 050901 (2015).

[5] R. Verba, V. Tiberkevich, and A. Slavin, Influence of interfacial Dzyaloshinskii-Moriya interaction on the parametric amplification of spin waves, Appl. Phys. Lett. **107**, 112402 (2015).

[6] E. Berrios-Caro, M. G. Clerc, and A. O. Leon, Flaming 2π kinks in parametrically driven systems, Phys. Rev. E **94**, 052217 (2016).

[7] V. Lauer, D. A. Bozhko, T. Brächer, P. Pirro, V. I. Vasyuchka, A. A. Serga, M. B. Jungfleisch, M. Agrawal, Yu. V. Kobljanskyj, G. A. Melkov, C. Dubs, B. Hillebrands, and A. V. Chumak, Spin-transfer torque based damping control of parametrically excited spin waves in a magnetic insulator, Appl. Phys. Lett. **108**, 012402 (2016).

[8] T. Brächer, P. Pirro, and B. Hillebrands, Parallel pumping for magnon spintronics: Amplification and manipulation of magnon spin currents on the micron-scale, Phys. Rep. **699**, 1 (2017).

[9] E. R. J. Edwards, H. Ulrichs, V. E. Demidov, S. O. Demokritov, and S. Urazhdin, Parametric excitation of magnetization oscillations controlled by pure spin current, Phys. Rev. B **86**, 134420 (2012).

[10] P. Bortolotti, E. Grimaldi, A. Dussaux, J. Grollier, V. Cros, C. Serpico, K. Yakushiji, A. Fukushima, H. Kubota, R. Matsumoto, and S. Yuasa, Parametric excitation of magnetic vortex gyrations in spin-torque nano-oscillators, Phys. Rev. B **88**, 174417 (2013).

[11] M. G. Clerc, S. Coulibaly, D. Laroze, A. O. Leon, and A. S. Nunez, Alternating spin-polarized current induces parametric resonance in spin valves, Phys. Rev. B **91**, 224426 (2015).

[12] D. Mancilla-Almonacid and R. E. Arias, Spin-wave modes in ferromagnetic nanodisks, their excitation via alternating currents and fields, and auto-oscillations, Phys. Rev. B **95**, 214424 (2017).

[13] D. Xiao, V. Tiberkevich, Y. H. Liu, Y. W. Liu, S. M. Mohseni, S. Chung, M. Ahlberg, A. N. Slavin, J. Akerman, and Y. Zhou, Parametric autoexcitation of magnetic droplet soliton perimeter modes, Phys. Rev. B **95**, 024106 (2017).

[14] P. Chowdhury, A. Jander, and P. Dhagat, Nondegenerate Parametric Pumping of Spin Waves by Acoustic Waves, IEEE Magn. Lett. **8**, 3108204 (2017).

[15] R. Verba, M. Carpentieri, G. Finocchio, V. Tiberkevich, and A. Slavin, Amplification and stabilization of large-amplitude propagating spin waves by parametric pumping, Appl. Phys. Lett. **112**, 042402 (2018).

[16] R. Verba, V. Tiberkevich, I. Krivorotov, and A. Slavin, Parametric Excitation of Spin Waves by Voltage-Controlled

Magnetic Anisotropy, Phys. Rev. Appl. **1**, 044006 (2014).

[17] R. Verba, M. Carpentieri, G. Finocchio, V. Tiberkevich, and A. Slavin, Excitation of propagating spin waves in ferromagnetic nanowires by microwave voltage-controlled magnetic anisotropy, Sci. Rep. **6**, 25018 (2016).

[18] Y-J. Chen, H. K. Lee, R. Verba, J. A. Katine, I. Barsukov, V. Tiberkevich, J. Q. Xiao, A. N. Slavin, and I. N. Krivorotov, Parametric Resonance of Magnetization Excited by Electric Field, Nano Lett. **17**, 572 (2017).

[19] B. Rana, Y. Fukuma, K. Miura, H. Takahashi, and Y. Otani, Excitation of coherent propagating spin waves in ultrathin CoFeB film by voltage-controlled magnetic anisotropy, Appl. Phys. Lett. **111**, 052404 (2017).

[20] R. Verba, M. Carpentieri, G. Finocchio, V. Tiberkevich, and A. Slavin, Excitation of Spin Waves in an In-Plane-Magnetized Ferromagnetic Nanowire Using Voltage-Controlled Magnetic Anisotropy, Phys. Rev. Appl. **7**, 064023 (2017).

[21] Y. Shiota, T. Maruyama, T. Nozaki, T. Shinjo, M. Shiraishi, and Y. Suzuki, Voltage-Assisted Magnetization Switching in Ultrathin $Fe_{80}Co_{20}$ Alloy Layers, Appl. Phys. Express **2**, 063001 (2009).

[22] Y. Suzuki, H. Kubota, A. Tulapurkar, and T. Nozaki, Spin control by application of electric current and voltage in FeCoMgO junctions, Philos. Trans. R. Soc. A **369**, 3658 (2011).

[23] T. Nozaki, Y. Shiota, S. Miwa, S. Murakami, F. Bonell, S. Ishibashi, H. Kubota, K. Yakushiji, T. Saruya, A. Fukushima, S. Yuasa, T. Shinjo, and Y. Suzuki, Electric-field-induced ferromagnetic resonance excitation in an ultrathin ferromagnetic metal layer, Nat. Phys. **8**, 491 (2012).

[24] S. Kanai, M. Yamanouchi, S. Ikeda, Y. Nakatani, F. Matsukura, and H. Ohno, Electric field-induced magnetization reversal in a perpendicular-anisotropy CoFeB-MgO magnetic tunnel junction, Appl. Phys. Lett. **101**, 122403 (2012).

[25] J. Zhu, J. A. Katine, G. E. Rowlands, Y. J. Chen, Z. Duan, J. G. Alzate, P. Upadhyaya, J. Langer, P. K. Amiri, K. L. Wang, and I. N. Krivorotov, Voltage-Induced Ferromagnetic Resonance in Magnetic Tunnel Junctions, Phys. Rev. Lett. **108**, 197203 (2012).

[26] D. Chiba, M. Sawicki, Y. Nishitani, Y. Nakatani, F. Matsukura, and H. Ohno, Magnetization vector manipulation by electric fields, Nat. Lett. **455**, 515 (2008).

[27] L. Gerhard, T. K. Yamada, T. Balashov, A. F. Takács, R. J. H. Wesselink, M. Däne, M. Fechner, S. Ostanin, A. Ernst, I. Mertig, and W. Wulfhekel, Magnetoelectric coupling at metal surfaces, Nat. Nanotechnol. **5**, 792 (2010).

[28] Y. Yamada, K. Ueno, T. Fukumura, H. T. Yuan, H. Shimotani, Y. Iwasa, L. Gu, S. Tsukimoto, Y. Ikuhara, and M. Kawasaki, Electrically Induced Ferromagnetism at Room Temperature in Cobalt-Doped Titanium Dioxide, Science **332**, 1065 (2011).

[29] A. Sekine and T. Chiba, Electric-field-induced spin resonance in antiferromagnetic insulators: Inverse process of the dynamical chiral magnetic effect, Phys. Rev. B **93**, 220403(R) (2016).

[30] A. O. Leon, A. B. Cahaya, and G. E. W. Bauer, Voltage Control of Rare-Earth Magnetic Moments at the Magnetic-Insulator Metal Interface, Phys. Rev. Lett. **120**, 027201 (2018).

[31] S. Miwa, M. Suzuki, M. Tsujikawa, K. Matsuda, T. Nozaki, K. Tanaka, T. Tsukahara, K. Nawaoka, M. Goto, Y. Kotani, T. Ohkubo, F. Bonell, E. Tamura, K. Hono, T. Nakamura, M. Shirai, S. Yuasa, and Y. Suzuki, Voltage controlled interfacial magnetism through platinum orbits, Nat. Commun. **8**, 15848 (2017).

[32] Q. Xiang, Z. Wen, H. Sukegawa, S. Kasai, T. Seki, T. Kubota, K. Takanashi, and S. Mitani, Nonlinear electric field effect on perpendicular magnetic anisotropy in Fe/MgO interfaces, J. Phys. D: Appl. Phys. **50**, 1361 (2017).

[33] Z. Wen, H. Sukegawa, T. Seki, T. Kubota, K. Takanashi, and S. Mitani, Voltage control of magnetic anisotropy in epitaxial Ru/Co2FeAl/ MgO heterostructures, Sci. Rep. **7**, 45026 (2017).

[34] Y. Shiota, T. Nozaki, S. Tamaru, K. Yakushiji, H. Kubota, A. Fukushima, S. Yuasa, and Y. Suzuki, Reduction in write error rate of voltage-driven dynamic magnetization switching by improving thermal stability factor, Appl. Phys. Lett. **111**, 022408 (2017).

[35] T. Yamamoto, T. Nozaki, Y. Shiota, H. Imamura, S. Tamaru, K. Yakushiji, H. Kubota, A. Fukushima, Y. Suzuki, and S. Yuasa, Thermally Induced Precession-Orbit Transition of Magnetization in Voltage-Driven Magnetization Switching, Phys. Rev. Appl. **10**, 024004 (2018).

[36] S. Tamaru, T. Yamamoto, T. Nozaki, and S. Yuasa, Accurate calculation and shaping of the voltage pulse waveform applied to a voltage-controlled magnetic random access memory cell, Jpn. J. Appl. Phys. **57**, 073002 (2018).

[37] A. Mougin, M. Cormier, J. P. Adam, P. J. Metaxas, and J. Ferre, Domain wall mobility, stability and Walker breakdown in magnetic nanowires, Europhys. Lett. **78**, 57007 (2007).

[38] S. S. P. Parkin, M. Hayashi, and L. Thomas, Magnetic Domain-Wall Racetrack Memory, Science **320**, 190 (2008).

[39] S. Wintz, V. Tiberkevich, M. Weigand, J. Raabe, J. Lindner, A. Erbe, A. Slavin, and J. Fassbender, Magnetic vortex cores as tunable spin-wave emitters, Nat. Nanotechnol. **11**, 948 (2016).

[40] K. Yamada, S. Kasai, Y. Nakatani, K. Kobayashi, H. Kohno, A. Thiaville, and T. Ono, Electrical switching of the vortex core in a magnetic disk, Nat. Mater. **6**, 270 (2007).

[41] V. S. Pribiag, I. N. Krivorotov, G. D. Fuchs, P. M. Braganca, O. Ozatay, J. C. Sankey, D. C. Ralph, and R. A. Buhrman, Magnetic vortex oscillator driven by d.c. spin-polarized current, Nat. Phys. **3**, 498 (2007).

[42] D. Kumar, S. Barman, and A. Barman, Magnetic Vortex Based Transistor Operations, Sci. Rep. **4**, 4108 (2014).

[43] O. Boulle, J. Vogel, H. Yang, S. Pizzini, D. de Souza Chaves, A. Locatelli, T. O. Mentes, A. Sala, L. D. Buda-Prejbeanu, O. Klein, M. Belmeguenai, Y. Roussigné, A. Stashkevich, S. M. Chérif, L. Aballe, M. Foerster, M. Chshiev, S. Auffret, I. M. Miron, and G. Gaudin, Room-temperature chiral magnetic skyrmions in ultrathin magnetic nanostructures, Nat. Nanotechnol. **11**, 449 (2016).

[44] N. Romming, A. Kubetzka, C. Hanneken, K. von Bergmann, and R. Wiesendanger, Field-Dependent Size and Shape of Single Magnetic Skyrmions, Phys. Rev. Lett. **114**, 177203 (2015).

[45] R. Wiesendanger, Nanoscale magnetic skyrmions in metallic films and multilayers: A new twist for spintronics, Nat. Rev. Mater. **1**, 16044 (2016).

[46] S. Woo, K. Litzius, B. Krüger, M.- Y. Im, L. Caretta, K. Richter, M. Mann, A. Krone, R. M. Reeve, M. Weigand, P. Agrawal, I. Lemesh, M.- A. Mawass, P. Fischer, M. Klaui, and

G. S. D. Beach, Observation of room-temperature magnetic skyrmions and their current-driven dynamics in ultrathin metallic ferromagnets, Nat. Mater. **15**, 501 (2016).

[47] P.- J. Hsu, A. Kubetzka, A. Finco, N. Romming, K. von Bergmann, and R. Wiesendanger, Electric-field-driven switching of individual magnetic skyrmions, Nat. Nanotechnol. **12**, 123 (2017).

[48] W. Jiang, P. Upadhyaya, W. Zhang, G. Yu, M. B. Jungfleisch, F. Y. Fradin, J. E. Pearson, Y. Tserkovnyak, K. L. Wang, O. Heinonen, S. G. E. te Velthuis, and A. Hoffmann, Blowing magnetic skyrmion bubbles, Science **349**, 283 (2015).

[49] D. D. Stancil and A. Prabhkar, *Spin Waves* (Springer, New York, 2008).

[50] See Supplemental Material at http://link.aps.org/supplemental/10.1103/PhysRevE.98.062213 for videos of the symmetric and asymmetric localized solutions.

[51] I. D. Mayergoyz, G. Bertotti, and C. Serpico, *Nonlinear Magnetization Dynamics in Nanosystems* (Elsevier, Oxford, 2009).

[52] O. Thual, S. Douady, and S. Fauve, Parametric Instabilities, in Book *Instabilities and Nonequilibrium Structures II*, edited by Enrique TirapeguiDanilo Villarroel (Springer, Dordrecht, 1989).

[53] M. Faraday, On a peculiar class of acoustical figures; and on certain forms assumed by groups of particles upon vibrating elastic surfaces, Philos. Trans. R. Soc. London **121**, 299 (1831).

[54] A. O. Leon, M. G. Clerc, and S. Coulibaly, Dissipative structures induced by spin-transfer torques in nanopillars, Phys. Rev. E **89**, 022908 (2014).

[55] J. Wu, R. Keolian, and I. Rudnick, Observation of a Nonpropagating Hydrodynamic Soliton, Phys. Rev. Lett. **52**, 1421 (1984).

[56] M. G. Clerc, S. Coulibaly, N. Mujica, R. Navarro, and T. Sauma, Soliton pair interaction law in parametrically driven Newtonian fluid, Philos. Trans. R. Soc. London A **367**, 3213 (2009).

[57] P. B. Umbanhowar, F. Melo, and H. L. Swinney, Localized excitations in a vertically vibrated granular layer, Nature (London) **382**, 793 (1996).

[58] M. G. Clerc, S. Coulibaly, M. A. Garcia-Nustes, and Y. Zarate, Dissipative Localized States with Shield-Like Phase Structure, Phys. Rev. Lett. **107**, 254102 (2011).

[59] M. Bondila, I. V. Barashenkov, and M. M. Bogdan, Topography of attractors of the parametrically driven nonlinear Schrödinger equation, Phys. D (Amsterdam) **87**, 314 (1995).

[60] M. G. Clerc, S. Coulibaly, and D. Laroze, Non-variational Ising-Bloch transition in parametrically driven systems, Int. J. Bifurcation Chaos **19**, 2717 (2009).

[61] I. V. Barashenkov and E. V. Zemlyanaya, Stable Complexes of Parametrically Driven, Damped Nonlinear Schrödinger Solitons, Phys. Rev. Lett. **83**, 2568 (1999).

[62] M. G. Clerc, S. Coulibaly, and D. Laroze, Parametrically driven instabilities in quasi-reversal systems, Int. J. Bifurcation Chaos **19**, 3525 (2009).

[63] A. O. Leon, Parametric Phenomena in Magnetic Nanostripes, Springer Proc. Phys. **173**, 247 (2016).

[64] I. V. Barashenkov, M. M. Bogdan, and V. I. Korobov, Stability diagram of the phase-locked solitons in the parametrically driven, damped nonlinear Schrödinger equation, Europhys. Lett. **15**, 113 (1991).

[65] D. Urzagasti, D. Laroze, M. G. Clerc, and H. Pleiner, Breather soliton solutions in a parametrically driven magnetic wire, Europhys. Lett. **104**, 40001 (2013).

[66] D. Anderson, M. Bonnedal, and M. Lisak, Self-trapped cylindrical laser beams, Phys. Fluids **22**, 1838 (1979).

[67] J. M. Hyman and B. Larrouturou, The numerical differentiation of discrete functions using polynomial interpolation methods, Appl. Math. Comp. **10**, 487 (1982).

[68] W. H Press, S. A Teukolsky, W. T. Vetterling, and B. P. Flannery, *Numerical Recipes in C*, Vol. 2 (Cambridge University Press, Cambridge, 1996).